Journal of Applied Physics

Internal resonance between the extensional and flexural modes in micromechanical resonators

Cite as: J. Appl. Phys. **126**, 164506 (2019); https://doi.org/10.1063/1.5115028
Submitted: 13 June 2019 . Accepted: 14 October 2019 . Published Online: 31 October 2019

Tianyi Zhang, Chaowei Guo, Zhuangde Jiang, and Xueyong Wei

Journal of Applied Physics | ARTICLE | scitation.org/journal/jap

Internal resonance between the extensional and flexural modes in micromechanical resonators

Cite as: J. Appl. Phys. **126**, 164506 (2019); doi: 10.1063/1.5115028
Submitted: 13 June 2019 · Accepted: 14 October 2019 ·
Published Online: 31 October 2019

Tianyi Zhang,[1] Chaowei Guo,[2] Zhuangde Jiang,[1] and Xueyong Wei[1,3,a)]

AFFILIATIONS

[1]State Key Laboratory for Manufacturing Systems Engineering, Xi'an Jiaotong University, Xi'an 710049, China
[2]State Key Laboratory for Mechanical Behavior of Materials, Xi'an Jiaotong University, Xi'an 710049, China
[3]State Key Laboratory of Applied Optics, Changchun Institute of Optics, Fine Mechanics and Physics, Chinese Academy of Sciences, Changchun 130033, China

[a)]**Electronic mail:** seanwei@mail.xjtu.edu.cn

ABSTRACT

Internal resonance between different vibration modes in micromechanical devices has been widely studied due to its promising application prospects in microelectromechanical systems (MEMS) resonators and oscillators. In this paper, we investigated the 2:1 internal resonance between the extensional and flexural modes in a micromechanical cantilever beam resonator using open and closed loop testing methods. In the open loop test, energy transfer from the extensional mode to the flexural mode induced by internal resonance is directly observed. Amplitude saturation and internal resonance bandwidth change in the extensional mode are experimentally studied and theoretically verified with numerical simulation. In the closed loop system, internal resonance produces a bistable self-oscillation frequency. The oscillation frequency of the extensional mode will be locked to one of the two peaks induced by internal resonance. In addition, obvious improvement in short-term frequency stability of the closed loop system is observed with the help of internal resonance. The dynamic characteristics studied in this research can be potentially used to enhance the performance of MEMS vibration devices by internal resonance.

I. INTRODUCTION

Microelectromechanical systems (MEMS) resonators and oscillators have drawn considerable attention due to their potential alternatives to quartz crystals in sensing, timing, frequency control, and other applications. Compared to quartz crystals, MEMS resonators and oscillators have shown significant advantages including low cost, small size, low power consumption, and integrability with CMOS processing.[1] Nonlinear mode coupling between different vibration modes, which is frequently observed in MEMS vibrating structure, has been studied for their potential to improve the performance of resonators and oscillators.[2–4] For instance, this mechanism can be used to adjust the nonlinear stiffness[3] or tune the resonance frequency[2] of a specific mode by controlling another vibration mode.

If the resonance frequencies of the coupled vibration modes satisfy an integer relationship, an extremely strong energy transfer will take place, leading to internal resonance.[5] The undriven vibration mode can draw energy from the directly driven mode and start to vibrate at a frequency which has an integer relationship with the vibrating frequency of the directly driven mode. Internal resonance can cause complicated dynamic phenomena and has been widely studied in recent years for its numerous potential applications.[6] A series of experimental investigations on internal resonance in MEMS vibrating devices have been proposed. The frequency ratio between the directly driven mode and internal resonance response mode can be 1:1,[7–9] 1:2,[7,10] 1:3,[11,12] 2:1,[13–18] 3:1,[16,19] and even 23:1.[20] Some extraordinary nonlinear dynamic characteristics induced by internal resonance have been studied: van der Avoort *et al.* studied the 2:1 internal resonance in a beam resonator and observed amplitude saturation in a higher frequency bulk mode.[13] Internal resonance in structures like the clamped-clamped beam (1:3),[11] H-shaped structure (2:1),[15] and square plate (23:1)[20] can also lead to amplitude saturation results. Antonio *et al.* tested a clamped-clamped beam resonator and observed frequency stability improvement by 1:3 internal resonance.[11] Similar

frequency stabilization phenomenon is also found in an arch beam resonator with a frequency ratio of 2:1 and 3:1.[21] It is believed that internal resonance has promising application prospects in MEMS resonators and oscillators.

Here, an investigation on the 2:1 internal resonance between the extensional and flexural modes in a micromechanical cantilever beam resonator is presented in this study. Open loop and closed loop tests of the internal resonance system are carried out. This paper is organized as follows: Sec. II describes a mathematical model of the 2:1 internal resonance system. Numerical simulation results of the open loop frequency response are shown in this section. Section III is devoted to picturing the micromechanical beam resonator design and the experimental testing method utilized in this study. The experimental results of the open loop and closed loop tests are shown in Sec. IV. In the open loop test, the extensional mode is directly driven by a frequency sweep signal. The frequency response of the extensional mode as well as the frequency spectrum of the flexural mode are measured to compare with the numerical simulation results in Sec. II. Then, in the closed loop test, the extensional mode is made to generate self-oscillations by a feedback control circuit. Self-oscillation frequency change and short-term frequency stability of the extensional mode are experimentally investigated with and without the existence of internal resonance.

II. RESONATOR MODELING

The extensional and flexural modes in a cantilever beam resonator are investigated in this paper. The beam resonator is schematically shown in Fig. 1. A stretching and a bending deformation in the cantilever beam correspond to the extensional and flexural vibration modes, respectively. The movement directions of the two modes are shown in red and blue arrows.

The system is modeled as two linear resonators coupled through quadratic nonlinear coefficients.[13,22] A set of equations of motion is shown as follows:

$$m_1\ddot{p} + m_1\omega_1^2 p = -d_1 p^2 - c_1\dot{p} - F\cos(\omega t), \tag{1}$$

$$m_2\ddot{q} + m_2\omega_2^2 q = -d_2 pq - c_2\dot{q}, \tag{2}$$

where m_1 and m_2 are equivalent mass of the extensional and flexural mode; p and q represent displacement of two vibration modes, respectively; ω_1 is resonance angular frequency of the extensional mode; ω_2 corresponds to the flexural mode; d_1 and d_2 are nonlinear coupling terms; c_1 and c_2 are model damping; F is driving force; and ω is driving angular frequency. The driving force is directly applied to the extensional mode, while the flexural mode is left undriven. The resonance frequency ratio of the extensional and the flexural mode is 2:1. A numerical simulation is operated based on the equations of motion using the Runge-Kutta method with the MATLAB ode45 function.

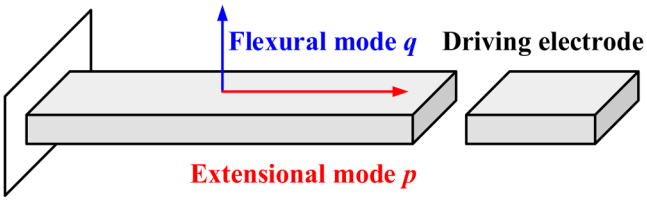

FIG. 1. Schematic of the cantilever beam resonator.

In numerical simulation, the frequency response of two modes is simulated by calculating their amplitude after the system reaches a steady state under certain driving conditions. The frequency response of the mode coupled system under different driving levels is shown in Figs. 2(a) and 2(b), corresponding to the extensional and flexural mode, respectively. The frequency response of the extensional mode shows a single resonance peak in a low driving force condition. Meanwhile, the flexural mode does not have any response, indicating that no energy exchange is observed when the driving force stays at a small value. A downward peak in the middle with two sharp upward peaks on both sides appears after the driving force exceeds a certain level, making the frequency response curve of the extensional mode look like a capital letter M. This unusual downward peak indicates that there exists energy leakage in the extensional mode. Meanwhile, the flexural mode shows a significant response as the driving frequency sweeps within the frequency range of the downward peak. The two upward peaks on both sides of the downward peak define an internal resonance bandwidth. This bandwidth marks the range in which the driving condition meets the internal resonance requirement. It should be noticed that the width of the internal resonance bandwidth is affected by the driving force, and the amplitude of the extensional mode at the downward peak almost stays constant. The amplitude of the extensional mode at this point as well as the internal resonance bandwidth are figured out as a function of the driving force. The results are shown in Fig. 2(c). The extensional mode shows an amplitude saturation (AS) phenomenon at the downward peak frequency after internal resonance occurs. The flexural mode draws extra energy to maintain this saturation in the extensional mode. Besides, the internal resonance bandwidth grows as the driving force increases, indicating that a stronger driving force creates a wider driving frequency range in which the internal resonance requirement is satisfied.

III. EXPERIMENTAL SETUP

A micromechanical cantilever beam resonator is designed and fabricated. The resonator fabricated by a standard silicon on insulator (SOI) process consists of two side-by-side microcantilever beams with mass blocks on their ends, as shown in Fig. 3(a). The two beams are identical with dimensions of 233 μm long, 10 μm wide, and 10 μm thick. A tiny silicon bar of 24 μm long and 4 μm wide is designed to connect two mass blocks in order to enable a current through the resonator body. Two small square blocks made of a platinum compound are deposited on the surface of each mass blocks by a focused ion beam (FIB) technique, which are used to adjust the resonance frequency of the extensional mode by changing its equivalent mass. The frequency ratio of the extensional and

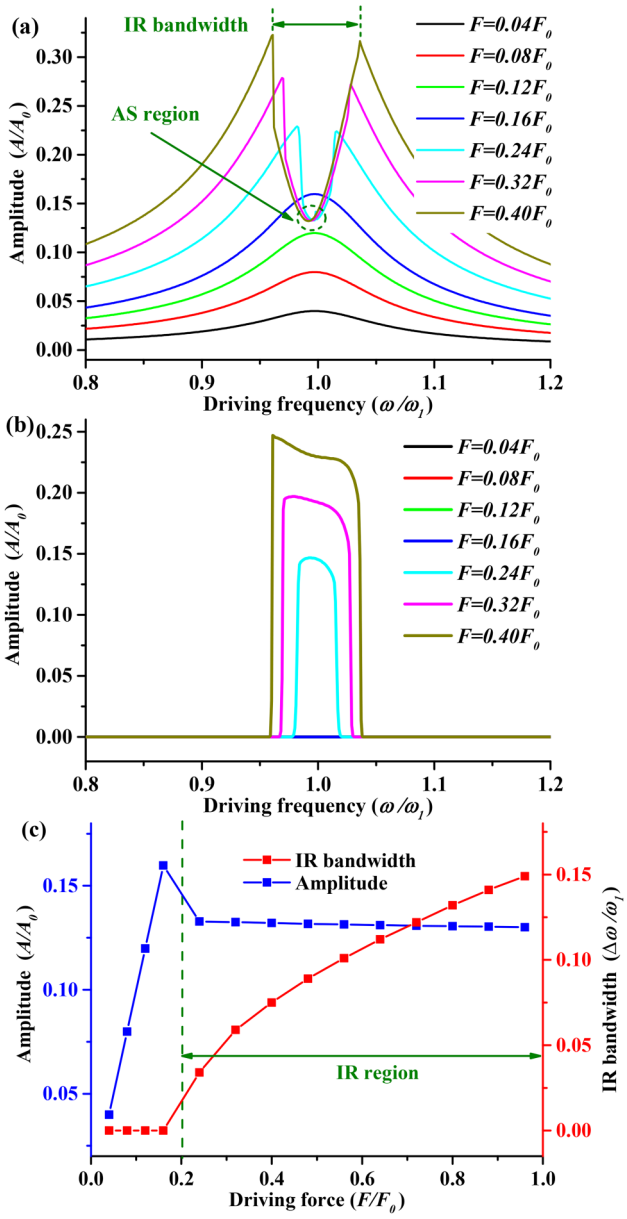

FIG. 2. Simulated frequency response of extensional (a) and flexural (b) modes. In (a), the green dashed lines label the internal resonance bandwidth, and the green dashed circle indicates the amplitude saturation point. (c) is the amplitude and IR bandwidth of the extensional mode as a function of driving force F. In this simulation, $\omega_1 = 2\omega_2 = 1\,\mathrm{s}^{-1}$, $d_1A_0/(m_1\omega_1^2) = 1$, $d_2A_0/(m_2\omega_2^2) = 0.6$, $c_1/(m_1\omega_1) = 0.1$, $c_2/(m_2\omega_2) = 0.04$, $A_0 = F_0/(\omega_1 c_1)$, $F_0/m_1 = 0.5\,\mathrm{m/s}^2$.

flexural mode can thus be turned to be extremely close to 2:1 by adjusting the thickness of the small square blocks.

The experimental setup is also shown in Fig. 3(a). Electrostatic actuation and differential piezoresistive sensing methods[23,24] are

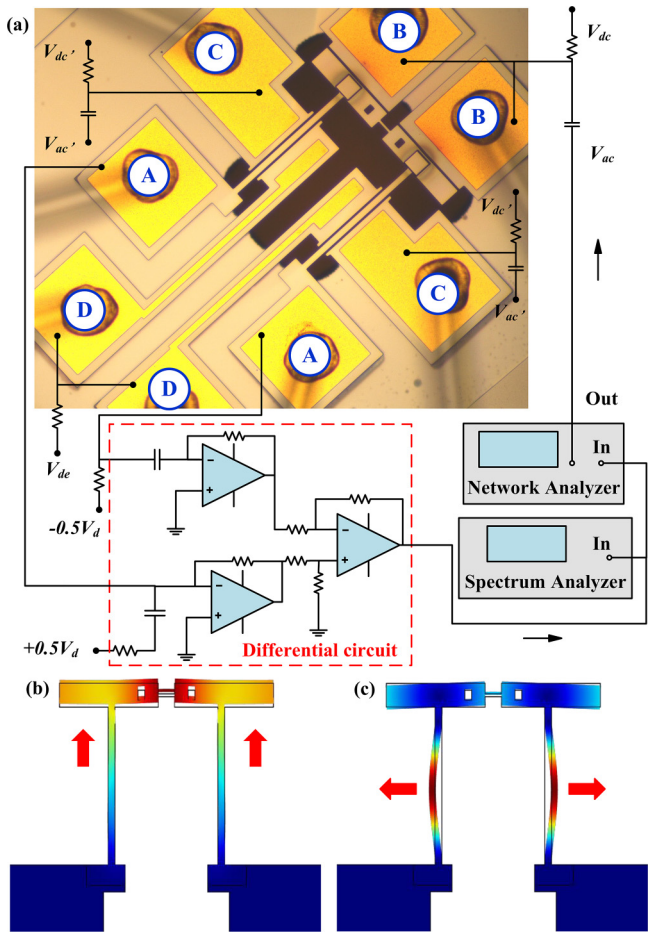

FIG. 3. (a) Microscopic picture and schematic of the open loop measurement setup of the micromechanical cantilever beam resonator. Mode shape of the extensional mode (b) and flexural mode (c) obtained by FEA simulation.

utilized in this experiment. The extensional mode is driven into vibration by a combination of V_{ac} and V_{dc} applied on two electrodes B. In order to characterize the flexural mode independently, $V_{ac'}$ and $V_{dc'}$ are also used on two electrodes C. The finite element analysis (FEA) simulated vibration mode shapes of these two modes are plotted in Figs. 3(b) and 3(c), respectively. Then, a differential pair of voltages $+0.5V_d$ and $-0.5V_d$ are separately applied on the two anchor pads A; therefore, a direct current is generated through the cantilever beam to facilitate differential piezoresistive sensing. The vibration of both extensional and flexural modes is sensed simultaneously by the piezoresistive effect without changing the readout port. The vibration signal is transformed into a voltage by a differential circuit and then collected by a network analyzer and a spectrum analyzer. Finally, a bias voltage V_{de} is applied on electrodes D to adjust the stiffness of the flexural mode through the electrostatic softening effect.[25] The testing system is placed in a vacuum chamber at a pressure below 0.02 Pa to

minimize the air-damping loss. The test is conducted in room temperature.

IV. EXPERIMENTAL RESULTS

A. Open loop tests

To begin with, the extensional mode and flexural mode are characterized separately in the open loop system. The frequency response curves of two modes under various driving forces are measured by a network analyzer, as shown in Figs. 4(a) and 4(b), respectively. The extensional mode has good linearity, while the flexural mode shows slight hardening nonlinearity. The resonance frequency ratio of the two modes is 1.9987 to 1 at a small amplitude. It should be noted that with a large driving force applied, a downward peak is observed in Fig. 4(a), indicating an amplitude drop and energy leakage in the extensional mode. The downward peak has a frequency twice the resonance frequency of the flexural mode, suggesting a 2:1 internal resonance between two vibration modes. The energy flows from the extensional mode to the flexural mode, leading to a downward internal resonance peak in the frequency response of the extensional mode.

To further confirm this judgment, a spectrum analyzer is used to measure the internal resonance response of the flexural mode during the process of the frequency response measurement in the extensional mode. The spectrum analyzer is set as maximum hold in each measurement. The frequency response of the extensional mode and the maximum frequency spectrum of the flexural mode are simultaneously measured under different V_{de} values. The results are shown in Fig. 5. The bias voltage V_{de} is utilized to adjust the stiffness of the flexural mode through electrostatic softening effect. Predictably, the resonance frequency of the flexural mode will drop

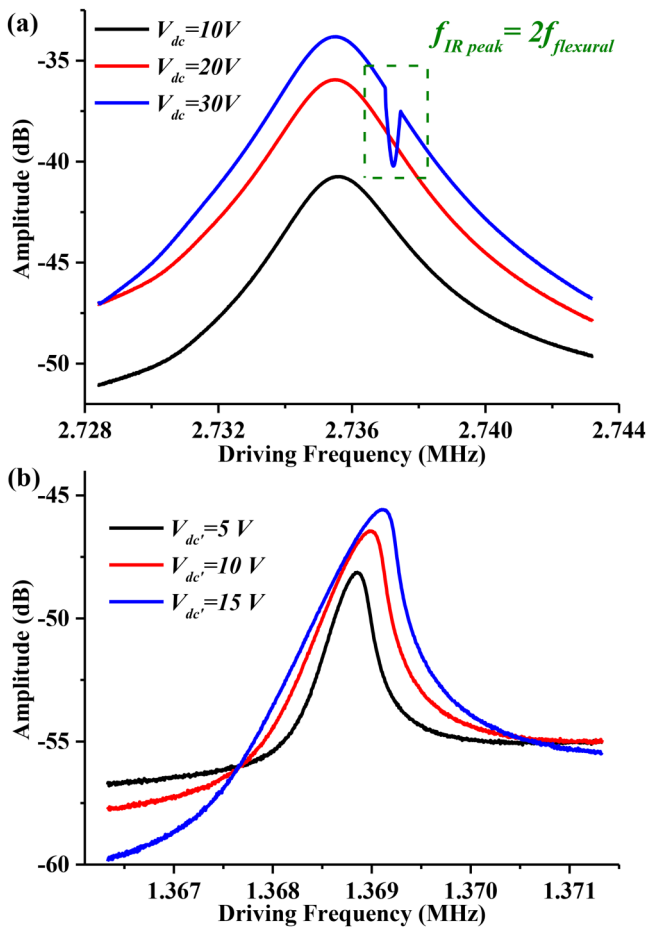

FIG. 4. Measured frequency response of the extensional (a) and flexural (b) mode separately under various driving forces. $V_{ac} = V_{ac'} = 10$ dbm, $V_d = 7$ V, $V_{de} = 0$ V in this experiment.

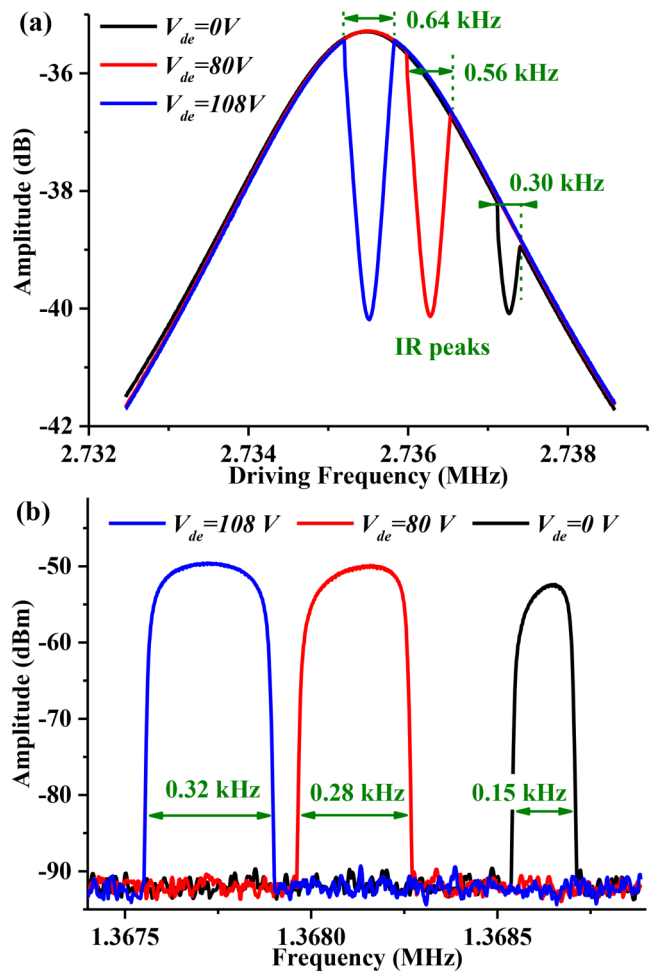

FIG. 5. Measured frequency response of the extensional mode with the network analyzer (a) and maximum frequency spectrum of the flexural mode with the spectrum analyzer (b). In (a), the green dashed lines label the internal resonance bandwidth of the extensional mode. $V_{ac} = 10$ dbm, $V_{dc} = 25$ V, $V_d = 7$ V, and $V_{ac'}$ and $V_{dc'}$ are idle.

as V_{de} increases. As can be found in Fig. 5(a), the downward internal resonance peak moves to lower frequency and approaches the resonance frequency of the extensional mode as V_{de} increases, which makes the resonance frequency ratio of two modes closer to 2:1. During this process, the IR peak becomes bigger and the IR bandwidth becomes wider, suggesting the internal resonance intensity becomes stronger as the resonance frequency ratio gets closer to an exact integer ratio. Meanwhile, during the frequency response measurement of the extensional mode, only when the driving frequency sweeps within the IR bandwidth can the response of the flexural mode be detected in the spectrum analyzer. The measured maximum frequency spectrum of the flexural mode in Fig. 5(b) and three IR peaks in Fig. 5(a) show an exact half frequency relationship, which fully corroborates the 2:1 internal resonance between the extensional and flexural mode.

Then, V_{de} is kept at 108 V as constant; thus, the frequency ratio of the two vibration modes is very close to 2:1. The frequency response of the extensional mode and the maximum frequency spectrum of the flexural mode are measured under various driving forces of the extensional mode. The results are shown in Fig. 6. As can be found in Fig. 6(a), the 2:1 internal resonance between the extensional and flexural mode suddenly appears when the driving force exceeds a certain level ($V_{dc} \geq 15$ V) and brings about a downward internal resonance peak with two upward peaks on its both sides. Meanwhile, in the maximum frequency spectrum of the flexural mode shown in Fig. 6(b), the internal resonance response of the flexural vibration becomes stronger and wider as the driving voltage of the extensional mode rises. Clear energy distribution of the extensional and flexural mode in the frequency domain under various driving conditions is observed, showing more energy transfers from the extensional mode to the flexural mode as the driving force increases. Attributed to such increasingly enhanced energy transfer, an amplitude saturation and IR bandwidth growth are detected in the extensional mode. The amplitude of the extensional mode at the IR peak point and the internal resonance bandwidth are figured out and plotted in Fig. 6(c). The amplitude of the extensional mode increases with the driving force in the beginning and then starts to saturate after internal resonance occurs. Meanwhile, the flexural mode draws extra energy, resulting in a wider IR bandwidth as the driving force increases. The results in Fig. 6 have a good agreement with the numerical simulation results in Fig. 2.

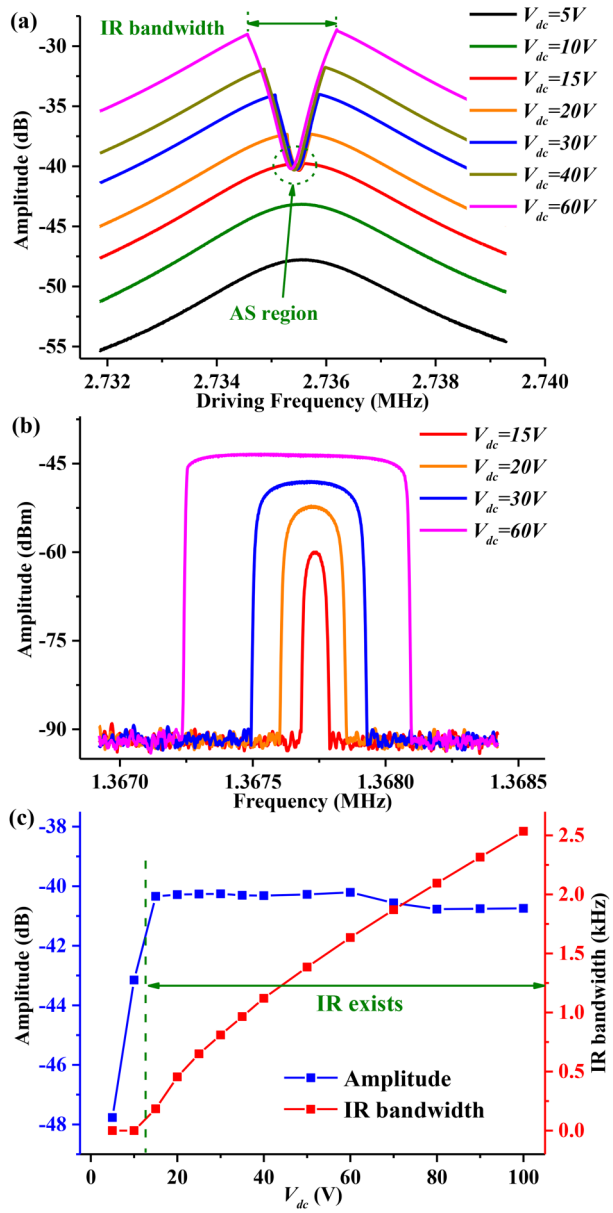

FIG. 6. Measured frequency response of the extensional mode with the network analyzer (a) and maximum frequency spectrum of the flexural mode with the spectrum analyzer (b) under various driving forces. In (a), the green dashed lines label the internal resonance bandwidth, and the green dashed circle indicates the amplitude saturation point. (c) is the amplitude and IR bandwidth of the extensional mode as a function of the driving voltage V_{dc}. In this experiment, $V_{ac} = 10$ dbm, $V_{de} = 108$ V, $V_d = 7$ V, and $V_{ac'}$ and $V_{dc'}$ are idle.

B. Closed loop tests

In this section, a closed loop feedback control circuit is utilized to make the extensional mode generate self-oscillation. The closed loop system is schematically shown in Fig. 7. The vibration signals of both extensional and flexural modes are collected by the differential circuit and delivered into an amplifier. Then, the extensional vibrating signal is selected by a bandpass filter and phase-shifted and finally transformed to a self-excitation driving signal V_{ac} by a gain controller. The closed loop oscillation frequency of the extensional mode is recorded by a frequency counter. Meanwhile, the vibration signal of the flexural mode is directly measured by a spectrum analyzer.

In the closed loop experiment, the resonance frequency of the flexural mode is set to be a variable parameter by adjusting V_{de}, and the self-oscillation frequency of the extensional mode is recorded. The oscillator is restarted each time after V_{de} changes in this measurement. The closed loop oscillation frequency of the extensional mode as a function of V_{de} is shown in the green line

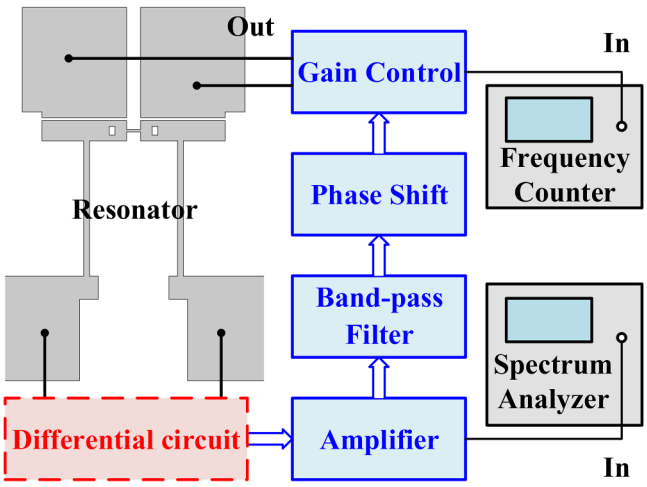

FIG. 7. Schematic of the closed loop measurement setup of the cantilever beam resonator.

labeled as "Direct" in Fig. 8(a). With the process of V_{de} gradually increasing from 30 V to 130 V, the output frequency barely changes in the beginning and then starts to drop when $V_{de} = 75$ V. This drop does not last long and is followed by a sudden jump to a higher frequency when $V_{de} = 95$ V. After that, the frequency again gradually drops close to the very beginning position at $V_{de} = 105$ V and then tends to be constant.

This self-oscillation frequency shifting phenomenon can be explained by introducing the frequency response of the extensional mode as shown in Figs. 8(b)–8(e), as well as the frequency spectrum of the flexural mode plotted in Figs. 8(f)–8(i). The frequency response is measured by breaking the connection between the phase shift and gain controller in Fig. 7 and inserting a network analyzer between them to operate the measurement. In the beginning, the bias voltage V_{de} is low, and the frequency of the IR peak is significantly higher than the resonance frequency of the extensional mode. The self-oscillation frequency of the extensional mode (marked in a red dashed line) locks to its original resonance peak as shown in Fig. 8(b). No internal resonance response of the flexural mode is observed as shown in Fig. 8(f). This part corresponds to region Non-IR 1 in Fig. 8(a). As V_{de} continues to increase, the IR peak moves to lower frequency. The oscillation frequency begins to lock to the upward peak on the left, as can be found in Fig. 8(c). Meanwhile, the flexural mode vibrates at exactly half of the extensional oscillation frequency due to 2:1 internal resonance [Fig. 8(g)]. The resonance frequency of the flexural mode drops as V_{de} increases because of the electrostatic softening effect; therefore, there exists a downtrend in the self-oscillation frequency of the extensional mode (IR-Low) in Fig. 8(a). Keeping V_{de} growing, then the oscillation frequency suddenly switches from the lower frequency upward peak to the higher frequency one [Fig. 8(d)], leading to a frequency jump. The system is still in internal resonance state [Fig. 8(h)], corresponding to region IR-High in Fig. 8(a). Similar downtrend of the oscillation frequency is observed

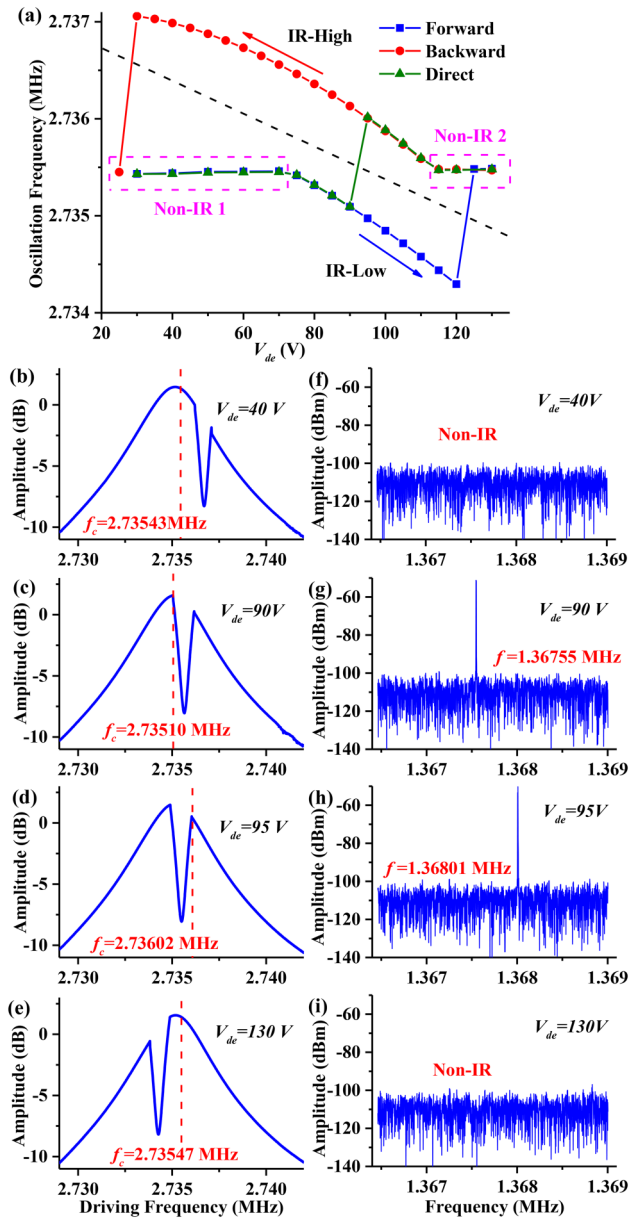

FIG. 8. (a) Measured closed loop oscillation frequency of the extensional mode as a function of V_{de}. (b)–(e) are frequency response curves of the extensional mode under different V_{de} values in the open loop test. The red dashed lines label the self-oscillation frequency of the extensional mode f_c. (f)–(i) are frequency spectra of the flexural mode under different V_{de} values in the closed loop system test. In the above measurement, $V_{dc} = 40$ V, $V_d = 7$ V, V_{ac} is constant depending on the gain control circuit, and $V_{ac'}$ and $V_{dc'}$ are idle.

due to the resonance frequency drop of the flexural mode. Finally, when V_{de} is too high and the frequency of the IR peak is significantly lower than the resonance frequency of the extensional mode, the self-oscillation frequency again locks back to the original

resonance peak of the extensional mode [Fig. 8(e)]. The internal resonance disappears [Fig. 8(i)]. Region Non-IR 2 in Fig. 8(a) shows this kind of situation. The internal resonance between the extensional and flexural mode leads to a downward IR peak with two sharp upward peaks on both sides in the open loop frequency response. When internal resonance occurs in the closed loop system, the self-oscillation frequency of the extensional mode will lock to one of the upward peaks in the frequency response. As for which the peak will be locked, it depends on the resonance frequency ratio between two vibration modes. The flexural mode will oscillate at the frequency exactly half of the extensional oscillation frequency. This mechanism enables integer multiple amplification of the resonance frequency shift of a certain vibration mode by measuring another mode in an internal resonance condition, which could be utilized in frequency tuning and sensing signal amplification.[26,27]

In the above experiment, the oscillator is manually restarted each time after V_{de} changes. Another two working conditions are considered in which the oscillator keeps working during the whole process. The self-oscillation frequency of the extensional mode as a function of the bias voltage V_{de} in these two conditions is also shown in Fig. 8(a). The blue and red lines correspond to the V_{de} forward and backward sweep, respectively. As can be seen in this figure, in the forward sweep condition, the oscillation frequency of the extensional mode always locks to the lower frequency upward peak during internal resonance exists, even at high V_{de} value (115–120 V) where internal resonance cannot exist in the former experiment. Meanwhile, if V_{de} sweeps backward, a similar phenomenon is observed that the self-oscillation frequency maintains at the higher frequency upward peak in the presence of internal resonance, and internal resonance will keep existing until a very low V_{de} value (30 V). The oscillation frequency of the extensional mode shows a bistable phenomenon and tends to stay at the first locked upward peak if the oscillator keeps working. This bistable oscillation frequency system also shows a hysteresis characteristic.

It is demonstrated that in a mode-coupled system, irregular vibration in one mode is transduced into frequency noise of another mode.[28,29] However, frequency stability can be improved when different modes satisfy an internal resonance condition.[11,21] In the final experiment, the frequency stability of the closed loop oscillator is experimentally studied by analyzing Allan deviation in non-IR and IR conditions. The bias voltage V_{de} is first set to be 0 V, and internal resonance is absent in the closed loop system. The self-oscillation frequency of the extensional mode in 500 s is recorded by a frequency counter with a gate time of 10 ms. Then, V_{de} is fixed at 95 V to make sure internal resonance occurs, and the output frequency is recorded again with the same settings. The oscillator is restarted before each measurement in this experiment. The Allan deviation as a function of integration time in two conditions is calculated, as shown in Fig. 9(a). It is found that the short-term frequency stability is improved if internal resonance exists. The improvement can be as large as one magnitude at an integration time of 100 s. To explain the frequency stabilization phenomenon, the amplitude and phase of the extensional mode as a function of driving frequency are measured by a network analyzer and plotted in Figs. 9(b) and 9(c), respectively. The measurement method is the same as the previous experiment shown in Fig. 8.

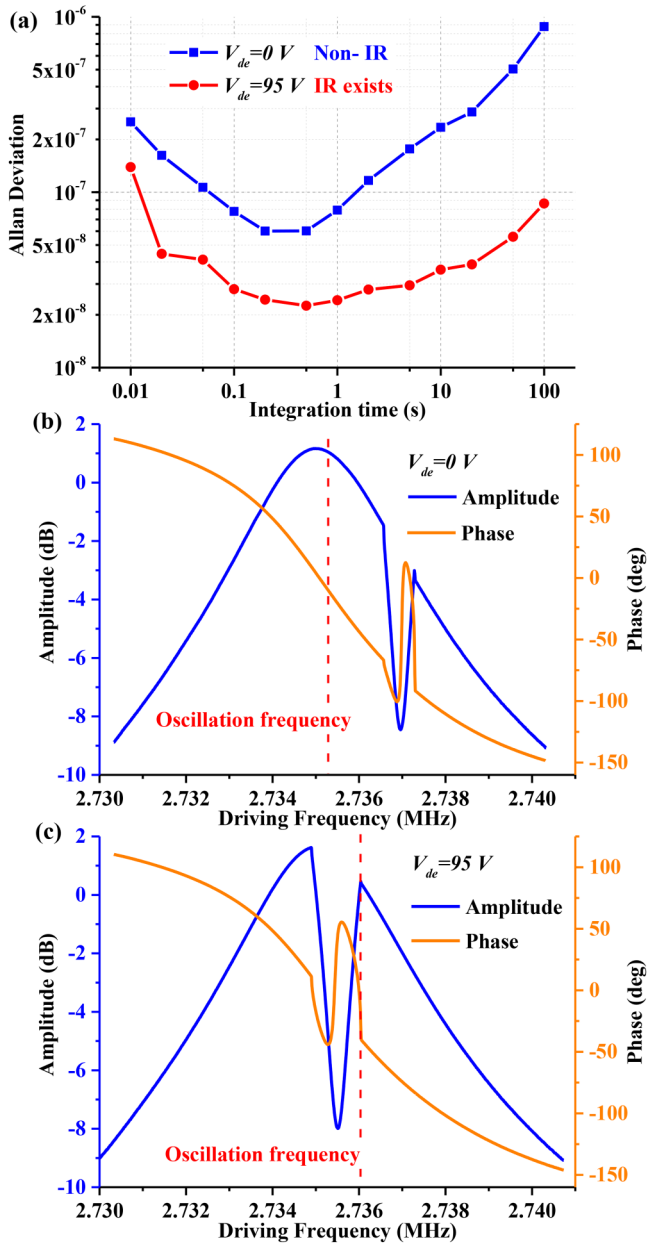

FIG. 9. (a) Allan deviation of the cantilever beam oscillator in non-IR and IR conditions. (b) and (c) are measured amplitude and phase response of the extensional mode in different frequency ratio conditions. $V_{dc} = 40$ V, $V_d = 7$ V, V_{ac} is constant depending on the gain control circuit, and $V_{ac'}$ and $V_{dc'}$ are idle in this experiment.

The closed loop oscillation frequency is marked with red dashed lines in these two figures. As can be seen in the non-IR condition, the oscillation frequency locks to the original resonance peak of the extensional mode, which corresponds to a gradual phase-frequency slope point (−0.0502°/Hz) in the phase response curve. However,

when internal resonance occurs, the oscillator will work at the frequency of the upward peak with higher frequency, corresponding to a very steep phase-frequency slope (−1.1609°/Hz). It is demonstrated in some publications that nonlinearity of a resonator leads to improved frequency stability when the phase shift of the sustaining amplifier forces the operating point to a steeper phase-frequency slope.[30,31] The internal resonance induced steep phase-frequency slope in the closed loop system reduces the influences of phase variations on the oscillation frequency; thus, a frequency stabilization is achieved. Such short-term frequency stability improvement induced by the internal resonance between two coupled vibration modes could be applied to a wide range of MEMS oscillators.

V. CONCLUSION

In this paper, the 2:1 internal resonance between the extensional and flexural mode in a micromechanical cantilever beam resonator is investigated. The mode-coupled system is first modeled by a quadratic nonlinear coupling equation set. The frequency response of the extensional and flexural modes is numerically simulated. Amplitude saturation and IR bandwidth growth are observed within the downward internal resonance peak in the simulation results. Then, the beam resonator is experimentally tested with open and closed loop methods. In the open loop test, the energy distribution of the extensional and flexural mode in the frequency domain is characterized under various resonance frequency ratios or driving force condition, which is achieved by simultaneously measuring the frequency response of the extensional mode and the frequency spectrum of the flexural mode. Downward internal resonance peaks are observed in the frequency response of the extensional mode. Amplitude saturation and IR bandwidth growth phenomena are also observed as the driving force of the extensional mode increases above a certain threshold. The open loop test results have a good agreement with the numerical simulation.

In the subsequent closed loop test, the extensional mode is controlled to generate self-oscillation. The oscillation frequency of the extensional mode is experimentally studied. When there is no internal resonance, the self-oscillation frequency locks to the original resonance peak of the extensional mode, with no flexural mode vibration being detected. Internal resonance in the closed loop system appears when the ratio of the extensional oscillation frequency to the resonance frequency of the flexural mode is extremely close to 2:1, leading to a bistable self-oscillation frequency of the extensional mode. The oscillation frequency of the extensional mode can be tuned by adjusting the resonance frequency of the flexural mode in the case of internal resonance, and this tuning process shows a hysteresis under the influence of the bistable self-oscillation frequency mechanism. In addition, the short-term frequency stability of the extensional mode is improved when the internal resonance occurs, which can be explained by a steeper phase-frequency slope at the self-oscillation frequency point in the phase response curve. The dynamic characteristics induced by internal resonance show great potential to improve the performance of MEMS resonators and oscillators.

ACKNOWLEDGMENTS

This work was financially supported by the National Key R&D Program of China (No. 2018YFB2002303), National Natural Science Foundation of China (NNSFC) (No. 51575439), Key Research and Development Program of Shaanxi Province (No. 2018ZDCXL-GY-02-03), and 111 Project (No. B12016). We also appreciate the support from the State Key Laboratory of Applied Optics and International Joint Laboratory for Micro/Nano Manufacturing and Measurement Technologies.

REFERENCES

[1] R. Abdolvand, B. Bahreyni, J. E.-Y. Lee, and F. Nabki, "Micromachined resonators: A review," Micromachines **7**, 160 (2016).
[2] H. Westra, H. Van der Zant, and W. Venstra, "Modal interactions of flexural and torsional vibrations in a microcantilever," Ultramicroscopy **120**, 41–47 (2012).
[3] P. Truitt, J. Hertzberg, E. Altunkaya, and K. Schwab, "Linear and nonlinear coupling between transverse modes of a nanomechanical resonator," J. Appl. Phys. **114**, 114307 (2013).
[4] Y. Yang, E. Ng, P. Polunin, Y. Chen, S. Strachan, V. Hong, C. H. Ahn, O. Shoshani, S. Shaw, M. Dykman *et al.*, "Experimental investigation on mode coupling of bulk mode silicon MEMS resonators," in *2015 28th IEEE International Conference on Micro Electro Mechanical Systems (MEMS)* (IEEE, 2015), pp. 1008–1011.
[5] S. Shaw, "Internal resonances in tiny structures: New results and practical applications," in ENOC 2017, June 25–30, 2017, Budapest, Hungary, pp. 1–2.
[6] K. Asadi, J. Yu, and H. Cho, "Nonlinear couplings and energy transfers in micro- and nano-mechanical resonators: Intermodal coupling, internal resonance and synchronization," Philos. Trans. R. Soc. A **376**, 20170141 (2018).
[7] C. Samanta, P. Yasasvi Gangavarapu, and A. Naik, "Nonlinear mode coupling and internal resonances in MoS_2 nanoelectromechanical system," Appl. Phys. Lett. **107**, 173110 (2015).
[8] X. Wei, T. Zhang, Z. Jiang, J. Ren, and R. Huan, "Frequency latching in nonlinear micromechanical resonators," Appl. Phys. Lett. **110**, 143506 (2017).
[9] X. Li, T. Ono, R. Lin, and M. Esashi, "Resonance enhancement of micromachined resonators with strong mechanical-coupling between two degrees of freedom," Microelectron. Eng. **65**, 1–12 (2003).
[10] R. Potekin, S. Dharmasena, H. Keum, X. Jiang, J. Lee, S. Kim, L. A. Bergman, A. F. Vakakis, and H. Cho, "Multi-frequency atomic force microscopy based on enhanced internal resonance of an inner-paddled cantilever," Sens. Actuators A Phys. **273**, 206–220 (2018).
[11] D. Antonio, D. H. Zanette, and D. López, "Frequency stabilization in nonlinear micromechanical oscillators," Nat. Commun. **3**, 806 (2012).
[12] C. Chen, D. H. Zanette, D. A. Czaplewski, S. Shaw, and D. López, "Direct observation of coherent energy transfer in nonlinear micromechanical oscillators," Nat. Commun. **8**, 15523 (2017).
[13] C. van der Avoort, R. van der Hout, J. Bontemps, P. Steeneken, K. Le Phan, R. Fey, J. Hulshof, and J. Van Beek, "Amplitude saturation of MEMS resonators explained by autoparametric resonance," J. Micromech. Microeng. **20**, 105012 (2010).
[14] A. Sarrafan, B. Bahreyni, and F. Golnaraghi, "Design and characterization of microresonators simultaneously exhibiting 1/2 subharmonic and 2:1 internal resonances," in *2017 19th International Conference on Solid-State Sensors, Actuators and Microsystems (TRANSDUCERS)* (IEEE, 2017), pp. 102–105.
[15] A. Sarrafan, B. Bahreyni, and F. Golnaraghi, "Development and characterization of an h-shaped microresonator exhibiting 2: 1 internal resonance," J. Microelectromech. Syst. **26**, 993–1001 (2017).
[16] A. H. Ramini, A. Z. Hajjaj, and M. I. Younis, "Tunable resonators for nonlinear modal interactions," Sci. Rep. **6**, 34717 (2016).

[17]A. Vyas, D. Peroulis, and A. K. Bajaj, "A microresonator design based on nonlinear 1: 2 internal resonance in flexural structural modes," J. Microelectromech. Syst. **18**, 744–762 (2009).
[18]N. Noori, A. Sarrafan, F. Golnaraghi, and B. Bahreyni, "Utilization of 2:1 internal resonance in microsystems," Micromachines **9**, 448 (2018).
[19]H. M. Ouakad, H. M. Sedighi, and M. I. Younis, "One-to-one and three-to-one internal resonances in MEMS shallow arches," J. Comput. Nonlinear Dyn. **12**, 051025 (2017).
[20]L. Lipiäinen, A. Jaakkola, K. Kokkonen, and M. Kaivola, "Nonlinear excitation of a rotational mode in a piezoelectrically excited square-extensional mode resonator," Appl. Phys. Lett. **100**, 153508 (2012).
[21]A. Hajjaj, N. Jaber, M. Hafiz, S. Ilyas, and M. Younis, "Multiple internal resonances in MEMS arch resonators," Phys. Lett. A **382**, 3393–3398 (2018).
[22]A. H. Nayfeh and D. T. Mook, *Nonlinear Oscillations* (John Wiley & Sons, 2008).
[23]X. Wei and A. A. Seshia, "Differential piezoresistive sensing in a bulk-mode micromechanical resonator," Micro Nano Lett. **8**, 107–110 (2013).
[24]A.-H. Lin, J.-Y. Lee, J. Yan, and A. Seshia, "Methods for enhanced electrical transduction and characterization of micromechanical resonators," Sens. Actuators A Phys. **158**, 263–272 (2010).
[25]M. Agarwal, S. A. Chandorkar, H. Mehta, R. N. Candler, B. Kim, M. A. Hopcroft, R. Melamud, C. M. Jha, G. Bahl, G. Yama *et al.*, "A study of electrostatic force nonlinearities in resonant microstructures," Appl. Phys. Lett. **92**, 4106 (2008).
[26]T. Zhang, X. Wei, Z. Jiang, and T. Cui, "Sensitivity enhancement of a resonant mass sensor based on internal resonance," Appl. Phys. Lett. **113**, 223505 (2018).
[27]X. Du, D. F. Wang, C. Xia, S. Isao, and R. Maeda, "Internal resonance phenomena in coupled ductile cantilevers with triple frequency ratio—Part II: A mass sensitivity amplification schemes," IEEE Sens. J. **14**, 5484–5492 (2019).
[28]A. Vinante, "Thermal frequency noise in micromechanical resonators due to nonlinear mode coupling," Phys. Rev. B **90**, 024308 (2014).
[29]O. Maillet, X. Zhou, R. Gazizulin, A. M. Cid, M. Defoort, A. D. Fefferman, O. Bourgeois, and E. Collin, "Non-linear frequency transduction of nanomechanical Brownian motion," Phys. Rev. B **96**, 165434 (2017).
[30]B. Sun, C. Zhao, G. Sobreviela-Falces, S. Du, F. Han, X. Zou, and A. Seshia, "Enhanced frequency stability in a non-linear MEMS oscillator employing phase feedback," in *2017 IEEE 30th International Conference on Micro Electro Mechanical Systems (MEMS)* (IEEE, 2017), pp. 1115–1117.
[31]M. Pardo, L. Sorenson, and F. Ayazi, "An empirical phase-noise model for MEMS oscillators operating in nonlinear regime," IEEE Trans. Circuits Syst. I Regul. Pap. **59**, 979–988 (2012).